Low-frequency approximation for high-order harmonic generation by a bicircular laser field

D. B. Milošević
Faculty of Science, University of Sarajevo, Zmaja od Bosne 35, 71000 Sarajevo, Bosnia and Herzegovina; Academy of Sciences and Arts of Bosnia and Herzegovina, Bistrik 7, 71000 Sarajevo, Bosnia and Herzegovina; and Max-Born-Institut, Max-Born-Strasse 2a, 12489 Berlin, Germany

(Received 25 August 2017; published 22 January 2018)

We present low-frequency approximation (LFA) for high-order harmonic generation (HHG) process. LFA represents the lowest-order term of an expansion of the final-state interaction matrix element in powers of the laser-field frequency ω. In this approximation the plane-wave recombination matrix element which appears in the strong-field approximation is replaced by the exact laser-free recombination matrix element calculated for the laser-field dressed electron momenta. First, we have shown that the HHG spectra obtained using the LFA agree with those obtained solving the time-dependent Schrödinger equation. Next, we have applied this LFA to calculate the HHG rate for inert gases exposed to a bicircular field. The bicircular field, which consists of two coplanar counter-rotating fields having different frequencies (usually ω and 2ω), is presently an important subject of scientific research since it enables efficient generation of circularly polarized high-order harmonics (coherent soft x rays). Analyzing the photorecombination matrix element we have found that the HHG rate can efficiently be calculated using the angular momentum basis with the states oriented in the direction of the bicircular field components. Our numerical results show that the HHG rate for atoms having p ground state, for higher high-order harmonic energies, is larger for circularly polarized harmonics having the helicity -1. For lower energies the harmonics having helicity $+1$ prevails. The transition between these two harmonic energy regions can appear near the Cooper minimum, which, in the case of Ar atoms, makes the selection of high-order harmonics having the same helicity much easier. This is important for applications (for example, for generation of attosecond pulse trains of circularly polarized harmonics).

DOI: 10.1103/PhysRevA.97.013416

I. INTRODUCTION

High-order harmonic generation (HHG) is one of the highly nonlinear processes that occurs when atoms are exposed to a strong laser field. In this process extreme ultraviolet and soft x-ray radiation is emitted. Being coherent and ultrashort, this radiation found a broad range of applications. We mention here seminal experimental papers [1,2] in which HHG was discovered (see also a recent viewpoint article [3] and a review article [4]) and numerous applications [5–14]. The HHG process was explained using the three-step model [15–17]: after ionization (first step), the laser-field-driven electron returns to the parent ion (second step) and recombines with it, emitting a high-order harmonic (third step).

The high-order harmonic spectrum can be calculated solving the time-dependent Schrödinger equation (TDSE). The disadvantage of this method is that it is time consuming and that it does not give insight into the physics of the problem. Strong-field approximation (SFA) [17] is an approximative quantum-mechanical theory which is in accordance with the above-mentioned three-step model. It is assumed that the laser field is strong and that the influence of the atomic potential can be neglected during the propagation and recombination steps. In the context of the present paper, it should be mentioned that the SFA for a bichromatic elliptically polarized field was formulated in Ref. [18], while the SFA for a bicircular field was analyzed in detail in Ref. [19]. More recently, a better theoretical model, the so-called quantitative rescattering theory, was formulated [20] (see also the review article [21]), according to which the HHG emission rate can be expressed as a product of a returning electron wave packet and the photorecombination differential cross section of the laser-free continuum electron back to the initial bound state. An analytical factorization formula for the HHG rate, which is related to the three-step semiclassical scenario, was presented in Ref. [22].

The above-mentioned factorization formulas are applicable also for other strong-field processes which include rescattering. This can be shown using the so-called low-frequency approximation (LFA). The LFA dates back to the 1973 seminal paper by Kroll and Watson [23]. We have introduced it for laser-assisted scattering in Refs. [24,25] (see also the review article [26]) and for high-order above-threshold ionization in Ref. [27] (see also the earlier paper [28] and the more recent article [29] and references therein). In the present paper we derive the LFA for the HHG process, show that the obtained spectra agree with those obtained solving the TDSE, and apply the LFA to the bicircular field configuration.

HHG by bicircular field is presently a hot topic in strong-field physics and attoscience (see, for example, Ref. [30]). A bicircular field is a combination of two coplanar counter-rotating circularly polarized laser fields with different frequencies. Using this field it is possible to generate very bright harmonics in the extreme ultraviolet. This field configuration was first considered in Refs. [31–35]. The SFA for this field was formulated in Refs. [19,36,37]. A renewed interest in exploring

HHG via bicircular field was stimulated by the experimental confirmation that the harmonics generated in such a field are circularly polarized [38], which is important for applications. After that a series of papers was published and this continues to be an important area of research [39–56].

In Sec. II we derive the low-frequency approximation for high-order harmonic generation. We also confirm its validity by comparison of the results obtained using the LFA with the results obtained by solving the TDSE. The photorecombination matrix element is analyzed in Sec. III. Section IV contains our numerical results for the HHG spectra. Finally, our concluding remarks are given in Sec. V. The atomic system of units (a.u.) is used.

II. LOW-FREQUENCY APPROXIMATION FOR HIGH-ORDER HARMONIC GENERATION

A. Definition of the harmonic intensity and bicircular field

The nth harmonic intensity, generated by a laser field with the electric field vector $\mathbf{E}(t)$ in the xy plane, defined by the unit vectors $\hat{\mathbf{e}}_x$ and $\hat{\mathbf{e}}_y$, is

$$I_n = \frac{(n\omega)^4}{2\pi c^3}\left(\left|T_n^x\right|^2 + \left|T_n^y\right|^2\right), \tag{1}$$

where

$$\mathbf{T}_n = T_n\hat{\mathbf{e}}_n = T_n^x\hat{\mathbf{e}}_x + T_n^y\hat{\mathbf{e}}_y = \int_0^T \frac{dt}{T}\sum_m \mathbf{d}_m(t)e^{in\omega t} \tag{2}$$

is the Fourier component of the time-dependent dipole. The nth harmonic is irradiated in the direction of the z axis and $\hat{\mathbf{e}}_n$ is the nth harmonic photon unit complex polarization vector. The laser field has period T and fundamental frequency $\omega = 2\pi/T$. Our ω–2ω bicircular field, with equal component intensities, $I = E_1^2 = E_2^2$, is defined by

$$\begin{aligned} E_x(t) &= [E_1\sin(\omega t) + E_2\sin(2\omega t)]/\sqrt{2}, \\ E_y(t) &= [-E_1\cos(\omega t) + E_2\cos(2\omega t)]/\sqrt{2}. \end{aligned} \tag{3}$$

As it is explained in Ref. [44], the sum over m in Eq. (2) is related to the active electrons, and the index m corresponds to the angular momentum basis. For atoms with closed electron shells and an outer electron configuration np^6 (Ne, Ar, Kr, and Xe atoms), in the spherical harmonics basis $Y_{1m}(\hat{\mathbf{r}})$, only the matrix elements with ground-state magnetic quantum number $m = \pm 1$ are different from zero. One can also use a different angular momentum basis, defined by

$$f_\pm(\hat{\mathbf{r}}) = [Y_{11}(\hat{\mathbf{r}}) \pm Y_{1-1}(\hat{\mathbf{r}})]/\sqrt{2}. \tag{4}$$

The state f_+ (f_-) is oriented along the direction of the x (y) axis.

B. Derivation of the LFA

The main result in Ref. [29] was a power expansion in the laser-field frequency ω whose lowest-order term we called the LFA. In the present context, this approximation is given by

$$\int d\tau G(t,\tau)V|\chi_{\mathbf{k}}(\tau)\rangle \overset{\text{LFA}}{=} G_V(E_{\mathbf{k}+\mathbf{A}(t)})V|\chi_{\mathbf{k}}(t)\rangle, \tag{5}$$

where $G(t,\tau)$ is the time-dependent total retarded Green's operator, which satisfies relations $[i\partial/\partial t - H(t)]G(t,\tau) = \delta(t-\tau)$ and $G(t,\tau) = 0$ for $t < \tau$, with $H(t) = -\nabla^2/2 + V(\mathbf{r}) + \mathbf{r}\cdot\mathbf{E}(t)$ the total Hamiltonian of the electron interacting with the atomic potential $V(\mathbf{r})$ and the laser electric field $\mathbf{E}(t)$ [interaction $\mathbf{r}\cdot\mathbf{E}(t)$ is in length gauge and dipole approximation]. $|\chi_{\mathbf{k}}(t)\rangle = e^{i\mathbf{A}(t)\cdot\mathbf{r}}|\mathbf{k}\rangle e^{-iS_{\mathbf{k}}(t)} = |\mathbf{k}+\mathbf{A}(t)\rangle e^{-iS_{\mathbf{k}}(t)}$ are the Volkov states, where $\mathbf{E}(t) = -d\mathbf{A}(t)/dt$, $dS_{\mathbf{k}}(t)/dt = [\mathbf{k}+\mathbf{A}(t)]^2/2$, and $|\mathbf{q}\rangle$ denotes a plane-wave ket vector such that $\langle\mathbf{r}|\mathbf{q}\rangle = (2\pi)^{-3/2}\exp(i\mathbf{q}\cdot\mathbf{r})$. The time-independent Green's operator $G_V(E) = [E + i\varepsilon + \nabla^2/2 - V(\mathbf{r})]^{-1}$, $\varepsilon \to 0^+$, is calculated at the energy $E_{\mathbf{k}+\mathbf{A}(t)} = [\mathbf{k}+\mathbf{A}(t)]^2/2$.

The explicit form of the mentioned power expansion in ω can be obtained using the method described in Sec. III B in Ref. [29]. In short, after the substitution $t' = t - \tau$, $\varphi = \omega t$, we get

$$\begin{aligned} &\int d\tau G(t,\tau)V|\chi_{\mathbf{k}}(\tau)\rangle \\ &= \int dt' \int \frac{dE}{2\pi} e^{-i[(E+i\varepsilon)t' + f(\mathbf{r},t)]} \\ &\quad\times \sum_{n=0}^{\infty}\omega^n\left[-i\Gamma(\varphi)\frac{\partial}{\partial\varphi}\right]^n \Gamma(\varphi)Ve^{if(\mathbf{r},t)}|\chi_{\mathbf{k}}(t-t')\rangle, \end{aligned} \tag{6}$$

where $\Gamma(\varphi) = e^{-i\mathbf{A}(t)\cdot\mathbf{r}}G_V(E_{\mathbf{k}+\mathbf{A}(t)})e^{i\mathbf{A}(t)\cdot\mathbf{r}}$ and $f(\mathbf{r},t) = S_{\mathbf{k}}(t) - \mathbf{A}(t)\cdot\mathbf{r} - Et$. The $n = 0$ term of this expansion leads to the LFA result [Eq. (5)].

Physically, approximation (5) means that the time-dependent dynamics of the electron in the presence of both the potential V and the laser field is such that the laser-driven electron velocity changes only little while the electron passes over a distance on the order of the range of the potential V. Therefore, the total Green's operator is replaced by the time-independent Green's operator in the absence of the laser field, $G(t,\tau) \to G_V(E_{\mathbf{k}+\mathbf{A}(t)})\delta(t-\tau)$, calculated at the laser-dressed energy $E_{\mathbf{k}+\mathbf{A}(t)}$. The range of validity of the LFA was estimated in Ref. [25] for a linearly polarized laser field. The maximum returned electron energy is of the order $E_p = p^2/2 = 3U_p$, where $U_p = A_0^2/4$ is the electron ponderomotive energy. For $p > A_0$ the small parameter of the LFA is $\frac{\hbar\omega}{E_p}\frac{2A_0}{p}$, while for $p < A_0$ it is $\hbar\omega/U_p = 4\omega^3/I$, with I the laser intensity, so that the LFA is valid not only for low frequencies but also for high intensities. For $p = A_0$ and the parameters used in the present paper this small parameter is from 0.065 for laser wavelength 800 nm and intensity 2×10^{14} W/cm^2 to 0.0075 for 1300 nm and 4×10^{14} W/cm^2. As in the case of the strong-field approximation, the exact range of validity of the LFA for highly nonlinear strong-field processes is difficult to determine. It should also be mentioned that the LFA is applicable to a multicolor elliptically polarized field [57].

Let us now show how the LFA affects the time-dependent dipole which appears in the S-matrix element of high-order harmonic generation (see Ref. [44] and references therein). We start from Eq. (9) from Ref. [44] (omitting indices a, i, and f):

$$\mathbf{d}(t) = \langle\psi(t)|\mathbf{r}\int dt' G(t,t')\mathbf{r}\cdot\mathbf{E}(t')|\psi(t')\rangle. \tag{7}$$

Introducing the Volkov Green's operator $G_{\rm le}(t,\tau) = -i\theta(t-\tau)\int d\mathbf{k}|\chi_{\mathbf{k}}(t)\rangle\langle\chi_{\mathbf{k}}(\tau)|$, with $\theta(t-\tau)=1$ for $t \geqslant \tau$ and $\theta(t-\tau)=0$ for $t<\tau$ and in length gauge, and using the integral equation $G(t,t') = G_{\rm le}(t,t') + \int d\tau G(t,\tau)V G_{\rm le}(\tau,t')$, we can rewrite Eq. (7) as

$$\mathbf{d}(t) = -i\langle\psi(t)|\mathbf{r}\int dt'\int d\mathbf{k}\Big[|\chi_{\mathbf{k}}(t)\rangle + \int d\tau G(t,\tau)V|\chi_{\mathbf{k}}(\tau)\rangle\Big] \times\langle\chi_{\mathbf{k}}(t')|\mathbf{r}\cdot\mathbf{E}(t')|\psi(t')\rangle. \quad (8)$$

In the LFA, which is given by Eq. (5), Eq. (8) reduces to

$$\mathbf{d}^{\rm LFA}(t) = -i\langle\psi(t)|\mathbf{r}\int dt'\int d\mathbf{k}[|\mathbf{k}+\mathbf{A}(t)\rangle + G_V(E_{\mathbf{k}+\mathbf{A}(t)})V|\mathbf{k}+\mathbf{A}(t)\rangle]e^{-iS_{\mathbf{k}}(t)} \times\langle\chi_{\mathbf{k}}(t')|\mathbf{r}\cdot\mathbf{E}(t')|\psi(t')\rangle. \quad (9)$$

Solutions $|\psi_{\mathbf{k}}\rangle$ of the stationary Schrödinger equation with the Hamiltonian $-\nabla^2/2 + V(\mathbf{r})$ satisfy the relation $|\psi_{\mathbf{k}}\rangle = |\mathbf{k}\rangle + G_V(E_{\mathbf{k}})V|\mathbf{k}\rangle$, so that we get

$$\mathbf{d}^{\rm LFA}(t) = -i\int dt'\int d\mathbf{k}\langle\psi(t)|\mathbf{r}|\psi_{\mathbf{k}+\mathbf{A}(t)}\rangle e^{-iS_{\mathbf{k}}(t)} \times\langle\chi_{\mathbf{k}}(t')|\mathbf{r}\cdot\mathbf{E}(t')|\psi(t')\rangle. \quad (10)$$

Our final result for the time-dependent dipole in the LFA is obtained after solving the integral over the intermediate electron momenta $\mathbf{k}$ using the saddle-point method. It is given by

$$\mathbf{d}_m^{\rm LFA}(t) = -i\left(\frac{2\pi}{i}\right)^{3/2}\int_0^\infty \frac{d\tau}{\tau^{3/2}}\langle\psi_m|\mathbf{r}|\psi_{\mathbf{k}_s+\mathbf{A}(t)}\rangle e^{iS_s} \times\langle\mathbf{k}_s+\mathbf{A}(t-\tau)|\mathbf{r}\cdot\mathbf{E}(t-\tau)|\psi_m\rangle, \quad (11)$$

where the index m denotes the magnetic quantum number of the ground state, and $S_s \equiv -I_p\tau - \int_{t-\tau}^t dt'[\mathbf{k}_s+\mathbf{A}(t')]^2/2$, with I_p the ionization potential and $\mathbf{k}_s = -\int_{t-\tau}^t dt'\mathbf{A}(t')/\tau$ the stationary momentum. This result is introduced into Eqs. (2) and (1) to calculate the harmonic intensity.

C. Comparison of the LFA and TDSE results for a linearly polarized laser pulse

In order to illustrate the validity of the LFA, in Fig. 1 we compare the LFA harmonic intensity (calculated in atomic units) and the TDSE harmonic intensity (TDSE data are obtained in arbitrary units and scaled by a constant factor). The total laser pulse duration is four optical cycles (upper panel) and seven optical cycles (lower panel). The results are for a hydrogen atom and a linearly polarized sine-squared few-cycle laser pulse with intensity 3×10^{14} W/cm^2, wavelength 800 nm, and carrier-envelope phase 105°. The notation of Ref. [58] is used. For an H atom in Eq. (11) we have $m=0$ and the matrix elements are calculated analytically. Agreement between the LFA and TDSE results in Fig. 1 is good, which confirms the validity of the LFA.

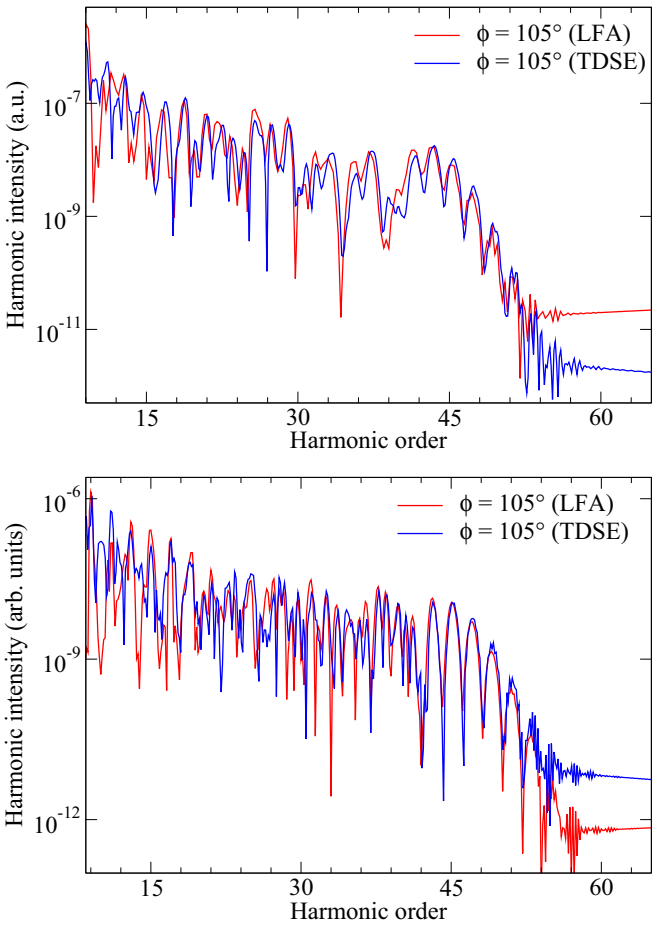

FIG. 1. Comparison of the harmonic intensity obtained using the LFA (red curves) and the TDSE (blue curves) for HHG by hydrogen atom and a linearly polarized few-cycle laser pulse with a sine-squared envelope, wavelength 800 nm, intensity 3×10^{14} W/cm^2, carrier-envelope phase 105°, and total pulse duration of four optical cycles (upper panel) and seven optical cycles (lower panel).

III. PHOTORECOMBINATION MATRIX ELEMENT

Based on the challenge imposed by experimental measurement of the atomic photoionization cross section in 1960s, the theory of atomic photoionization has advanced rapidly [59,60]. More recently, in the context of HHG the calculation of the photoionization amplitude by simple methods has again become important. Namely, the third step of the HHG process is the recombination of the ionized electron with the parent ion followed by emission of a high-energy photon. The photorecombination and photoionization cross sections are closely related and can be calculated using the same methods. In particular, the observation of the Cooper minimum [61] in HHG spectra has attracted a lot of attention [20,62–65]. In this context, it was necessary to calculate the recombination amplitude beyond the strong-field approximation [66]. In this section we show how the recombination amplitude in Eq. (11), $\langle\psi_m|\mathbf{r}|\psi_{\mathbf{q}}\rangle$, with $\mathbf{q} = \mathbf{k}_s + \mathbf{A}(t)$, can be calculated.

We are using the single-active-electron approximation. Both the continuum state $\psi_{\mathbf{p}}^{(-)}$ and the bound state ψ_m are the eigenstates of the Hamiltonian $-\nabla^2/2 + V(r)$, where $V(r) = V_C(r) + V_s(r)$ with $V_C = -1/r$ the Coulomb potential and

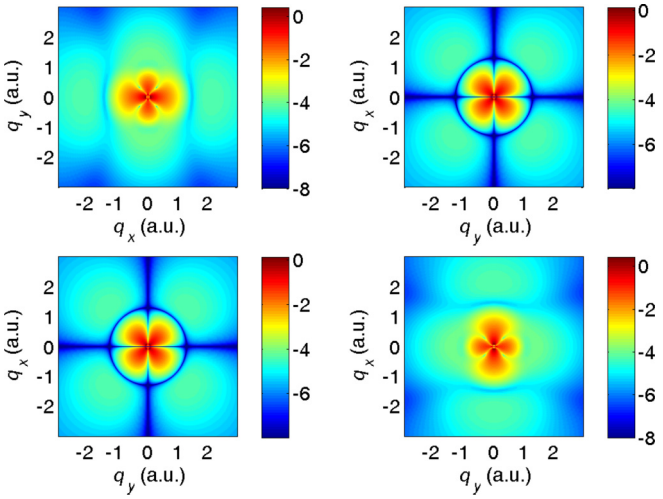

FIG. 2. Logarithm of the differential photorecombination cross sections for Ar, $|D^j_\pm|^2$ (in a.u.), with $j = x$ (y) for upper (lower) panels and "−" ("+") for left (right) panels, presented in false color in the momentum plane.

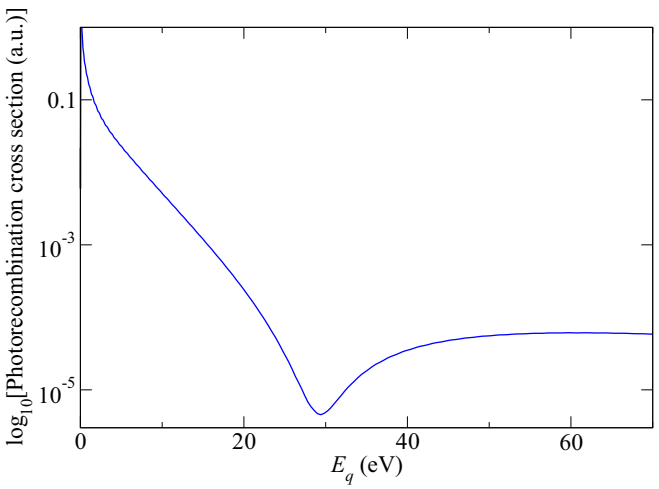

FIG. 3. Logarithm of the differential photorecombination cross sections for Ar as a function of the electron energy E_q for the f_- state and $\varphi_q = 0$ (see the upper left panel of Fig. 2).

$V_s(r)$ the short-range potential. The explicit form of the potential $V_s(r)$ is given by

$$V_s(r) = -(a_1 e^{-a_2 r} + a_3 r e^{-a_4 r} + a_5 e^{-a_6 r})/r, \tag{12}$$

where the coefficients a_j are tabulated in Ref. [67].

The bound-state wave function ψ_m is the wave function of the outer (valence) electron of the atom. We approximate it by the Hartree-Fock-type wave function, which is given in analytical form as a series expansion in atomic Slater-type orbitals:

$$\psi_m(\mathbf{r}) = \sum_a C_a N_a \varphi_{n_a l m}(\mathbf{r}), \quad N_a = \frac{(2\zeta_a)^{n_a+1/2}}{\sqrt{(2n_a)!}},$$
$$\varphi_{n_a l m}(\mathbf{r}) = r^{n_a-1} e^{-\zeta_a r} Y_{lm}(\hat{\mathbf{r}}), \tag{13}$$

where $Y_{lm}(\hat{\mathbf{r}})$ are spherical harmonics, $n_a l$ are the quantum numbers of the electron, and the parameters C_a, N_a, and ζ_a characterize the radial distribution of the electron density. For the inert gases Ne, Ar, Kr, and Xe, these parameters are tabulated in Ref. [68] and it is $l = 1$. For these states the ionization matrix elements $\langle \mathbf{q}'|\mathbf{r}\cdot\mathbf{E}(t-\tau)|\psi_m\rangle = i\mathbf{E}(t-\tau)\cdot\partial\tilde{\psi}_m(\mathbf{q}')/\partial\mathbf{q}'$, with $\tilde{\psi}_m(\mathbf{q}')$ the Slater-type orbitals in the momentum space and $\mathbf{q}' = \mathbf{k}_s + \mathbf{A}(t-\tau)$, are calculated analytically [44].

It is more complicated to calculate the recombination matrix elements, $\langle\psi_m|\mathbf{r}|\psi^{(-)}_{\mathbf{q}}\rangle$, with $\mathbf{q} = \mathbf{k}_s + \mathbf{A}(t)$. The continuum wave function $\psi^{(-)}_{\mathbf{p}}$ can be expanded as [59]

$$\psi^{(-)}_{\mathbf{q}}(\mathbf{r}) = \sqrt{\frac{2}{\pi}} \sum_{l,m} i^l R_{ql}(r) e^{-i(\sigma_l+\delta_l)} Y^*_{lm}(\hat{\mathbf{q}}) Y_{lm}(\hat{\mathbf{r}}), \tag{14}$$

where $Y_{lm}(\hat{\mathbf{q}}) \equiv Y_{lm}(\theta_q,\varphi_q)$ are spherical harmonics in momentum space, $\sigma_l(q) = \arg\Gamma(l+1-i/q)$ are the Coulomb phase shifts, while the (lth partial wave) phase shifts $\delta_l(q)$ [due to the short-range part of the potential $V(r)$] can be calculated numerically [69]. The continuum radial wave functions $R_{ql}(r)$, $q \equiv |\mathbf{q}|$, for fixed energy $E_{\mathbf{q}} = q^2/2$, can be calculated solving the radial Schrödinger equation with the potential $V(r)$ [69]. The normalization $\langle\psi^{(-)}_{\mathbf{q}}|\psi^{(-)}_{\mathbf{q}'}\rangle = \langle\mathbf{q}|\mathbf{q}'\rangle = \delta(\mathbf{q}-\mathbf{q}')$ is used. The angular part of the integral in the recombination matrix element $D^j_m(q,\varphi_q) \equiv \langle\psi_m|j|\psi^{(-)}_{\mathbf{q}}\rangle$, $j = x,y$, can be calculated analytically. Introducing the notation

$$\mathcal{R}_{ql} = \frac{-e^{-i(\sigma_l+\delta_l)}}{2\pi\sqrt{3}} \sum_a C_a N_a \int_0^\infty dr r^{n_a+2} e^{-\zeta_a r} R_{ql}(r), \tag{15}$$

we obtain

$$D^x_m = m\mathcal{R}_{q0} - \frac{m}{2}\mathcal{R}_{q2}(3e^{-i2m\varphi_q} + 1), \tag{16}$$

$$D^y_m = -i\mathcal{R}_{q0} - \frac{i}{2}\mathcal{R}_{q2}(3e^{-i2m\varphi_q} - 1). \tag{17}$$

The corresponding matrix elements in the basis $\sqrt{2}f_\pm$ are

$$D^x_+ = -i\,D^y_- = 3i\mathcal{R}_{q2}\sin(2\varphi_q), \tag{18}$$

$$D^x_- = 2\mathcal{R}_{q0} - \mathcal{R}_{q2}[1 + 3\cos(2\varphi_q)], \tag{19}$$

$$D^y_+ = -i\{2\mathcal{R}_{q0} - \mathcal{R}_{q2}[1 - 3\cos(2\varphi_q)]\}. \tag{20}$$

We calculated the differential photorecombination cross sections, $|D^j_\pm|^2$, $j = x,y$, for Ar atoms and presented them in Fig. 2 in false colors in the momentum plane $(q_x,q_y) = (q\cos\varphi_q, q\sin\varphi_q)$. All results exhibit reflection symmetry with respect to the q_x and q_y axes. We also have $\int_0^{2\pi} d\varphi_q D^x_+ = \int_0^{2\pi} d\varphi_q D^y_- = 0$. The partial differential cross section along the x axis and with the f_- state (upper left panel) has the q_x axis ($\varphi_q = 0$) as a characteristic axis. The Cooper minima appear near the energy 30 eV along this axis. This is clearly seen in Fig. 3. Analogously, for the partial differential cross section along the y axis and with the f_+ state (lower right panel), the q_y axis ($\varphi_q = 90^\circ$) is important. We use this fact to simplify our numerical calculations of the HHG spectra. The above-mentioned symmetries are more visible if we calculate the ratio of the differential photorecombination cross

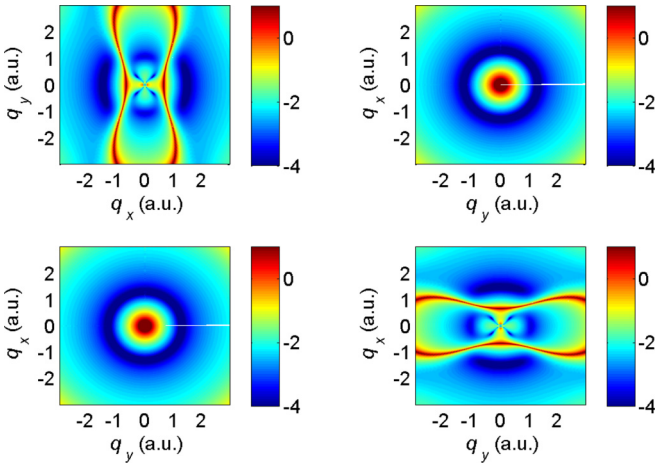

FIG. 4. Logarithm of the ratio of the differential photorecombination cross sections for exact and plane-wave continuum states, presented similarly as in Fig. 2.

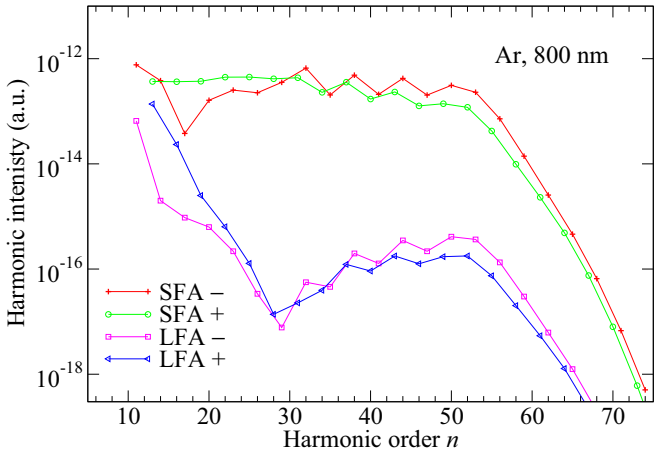

FIG. 5. Harmonic intensity for Ar and bicircular field with component wavelengths 800 and 400 nm and equal component intensities 4×10^{14} W/cm^2. The two upper curves are obtained using the strong-field approximation, while the two lower curves are calculated in the LFA.

sections obtained using the exact continuum wave functions and the corresponding sections obtained using the plane-wave continuum states, $\langle\psi_m|j|\mathbf{q}\rangle$ (plane waves are used in the standard SFA). This is presented in Fig. 4. The maxima which are almost parallel to the q_y (q_x) axis for the upper left (lower right) panel are related to the minima in the plane-wave cross sections. One can also notice that for fixed energy E_q the cross section in the upper left (lower right) panel is almost constant in a wide range around the angle $\varphi_q = 0^\circ$ ($\varphi_q = 90^\circ$). The importance of the angular momentum basis $f_\pm$ was noticed in Refs. [70–72], which consider HHG by an elliptically polarized laser field, and in Ref. [73] for a two-color laser field having orthogonal linear polarizations.

IV. NUMERICAL RESULTS FOR THE HHG SPECTRA BY BICIRCULAR FIELD

Numerical calculation of the harmonic intensity includes calculation of the double integral over the recombination time t and the travel time τ of highly oscillatory functions. In addition, we have to solve the radial Schrödinger equation, find exact radial continuum wave functions $R_{ql}(r)$ and phases σ_l and δ_l, as well as calculate numerically the integral over the radial coordinate r in Eq. (15). The problem can be simplified if we can withdraw the recombination matrix element in front of the integrals over time. Since the electron velocity at the recombination time, $\mathbf{q} = \mathbf{k}_s + \mathbf{A}(t)$, depends both on time t and time τ, this can be done only approximately. Applying the saddle-point method to the integral over the recombination time t in the Fourier component $\mathbf{T}_n$, Eq. (2), of the time-dependent dipole matrix element $\mathbf{d}(t)$, Eq. (11), we obtain the energy-conservation condition

$$n\omega = I_p + \mathbf{q}^2/2. \tag{21}$$

Therefore, the dominant contribution to the nth harmonic intensity comes from the momenta $q = \sqrt{2(n\omega - I_p)}$. This simplifies calculations since then the radial part of the recombination matrix element does not depend on the times t and τ. Furthermore, if we calculate the recombination matrix element in the basis $f_\pm$ then we can also fix φ_q to $\varphi_q = 0$ for f_- and to $\varphi_q = 90^\circ$ for f_+. The results presented in Figs. 2 and 4 justify this approximation. Having also in mind that our bicircular field is in the xy plane, we have $\theta_q = 90^\circ$. Therefore, not only the amplitude but also the orientation of the vector $\mathbf{q}$ can be fixed so that the complete recombination matrix element can be factorized out of the integrals over t and τ. The introduced additional approximations reduce the range of applicability of our LFA. The saddle-point approximation was also used in Ref. [25], where it led to the so-called on-shell LFA in which the matrix elements are calculated on the energy shell; i.e., the energy-conservation condition like Eq. (21) is satisfied. In this case the small parameter is estimated to be $\max\{\omega^2/\sqrt{I},\omega\}$, which is smaller than 0.06 in our examples.

In our numerical code we leave the strong-field approximation recombination matrix element inside the integrals over t and τ, but we multiply the obtained result by the square root of the ratio of the LFA and strong-field-approximation photorecombination cross sections for the corresponding matrix element in the basis $f_\pm$. In this way we avoid the influence of the phase of the LFA recombination matrix element which may change the phase of the subintegral function in wrong way since we have fixed φ_q. A proper way of taking into account this phase would be to solve the integral over time using the saddle-point method as in Ref. [27]. In this case the time becomes complex and additional approximation would be to neglect the small imaginary part of the recombination time t and of $\mathbf{k}_s$ (this is necessary since the code for calculation of the recombination amplitude works only for real momenta).

In Figs. 5 and 6 we show examples of the HHG spectra for Ar atoms, $\omega-2\omega$ bicircular field, and fixed component intensities. For Fig. 5, since the photon energy for 800 nm is $\omega = 1.55$ eV and minima appear for $n \approx 30$ we confirm the role of the Cooper minimum for Ar. Namely, for the Cooper minimum energy near 30 eV the harmonic energy is $I_p + q^2/2 = 15.76$ eV $+ 30$ eV $= 45.76$ eV $\approx 30\omega = 46.5$ eV [74]. Analogously, for Fig. 6 we have $I_p + q^2/2 \approx 48\omega$. Such minima are absent for the SFA results (two upper curves in Figs. 5

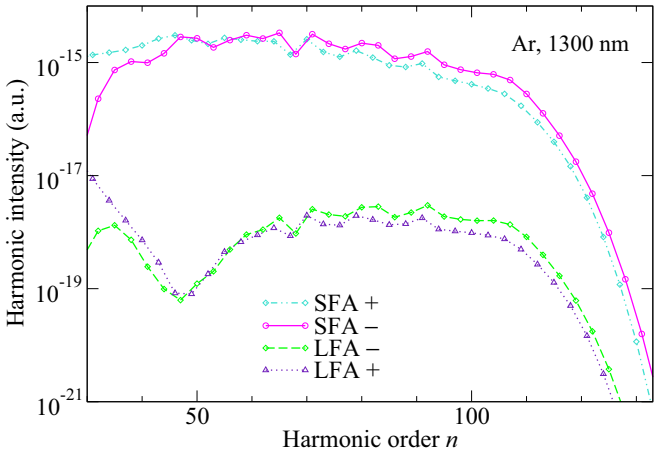

FIG. 6. Same as in Fig. 5 but for component wavelengths 1300 and 650 nm and equal component intensities 2×10^{14} W/cm^2.

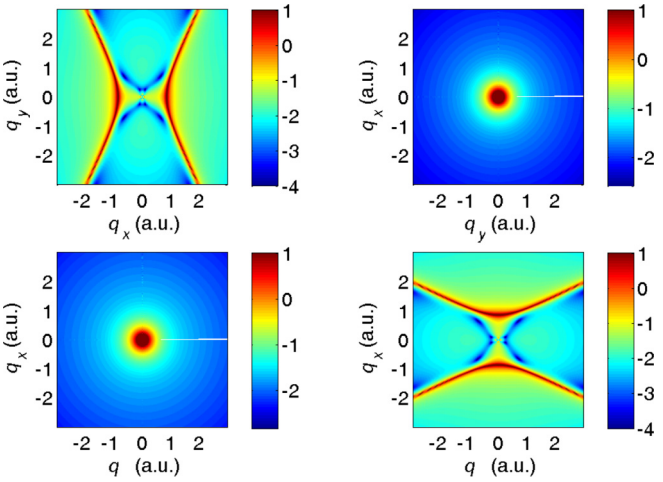

FIG. 8. Same as in Fig. 4 but for Ne atoms.

and 6). From Figs. 5 and 6 we see that the harmonic helicity inversion happens after the Cooper minimum. The harmonics having helicity -1 are stronger. This can be explained using the SFA theory as it has been done in Ref. [44] using the $m = \pm 1$ asymmetry.

In Fig. 7 we presented focal-averaged harmonic intensity as a function of the photon energy on a linear scale. The focal-averaged spectrum is obtained by integration from $0.3I_0$ to $0.999I_0$ harmonic intensity multiplied by the factor $\sqrt{I_0 - I}(2I + I_0)/I^{5/2}$. This factor was used before for focal averaging of the electron spectra [75]. Our method of focal averaging is approximate since we neglect the pulse shape and depletion effects [67]. From Fig. 7 it is clear that after the Cooper minimum the harmonics of helicity -1 are dominant. This fact can be used to generate an attosecond pulse train of circularly polarized harmonics. Let us clarify this. In Ref. [37] it was shown that by combining a group of bicircular-field-generated harmonics having alternating positive and negative helicity we can generate, during one driving-field cycle, three approximately linearly polarized pulses, which are rotated with respect to each other by 120° (this is experimentally confirmed in Ref. [30]). Further, in Ref. [42] it was shown that for atoms having the p ground state (the example of Ne atoms was used) the polarization of the generated attosecond pulses is close to elliptical due to the different intensities of the combined high-order harmonics of the opposite helicity. The harmonics having negative helicity are stronger at the end of the plateau and in the cutoff region, while the harmonics having positive helicity are stronger at the beginning of the plateau. If the transition between the mentioned regions in which positive or negative helicity harmonics are dominant happens near the Cooper minimum, this effect is enhanced as it is shown in Fig. 7. Therefore, combining a group of harmonics after the Cooper minimum, it is possible to generate an almost circularly polarized attosecond pulse train.

Let us now consider HHG by Ne atoms. From Fig. 8, which is an analog of Fig. 4, we see that in the case of Ne we do not have a characteristic Cooper-like minimum. As a consequence,

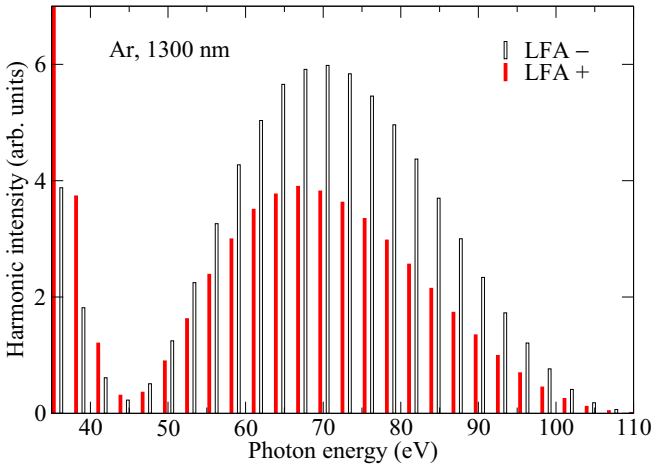

FIG. 7. Focal-averaged harmonic intensity for Ar and bicircular field with component wavelengths 1300 and 650 nm and equal component peak intensities $I_0 = 2 \times 10^{14}$ W/cm^2.

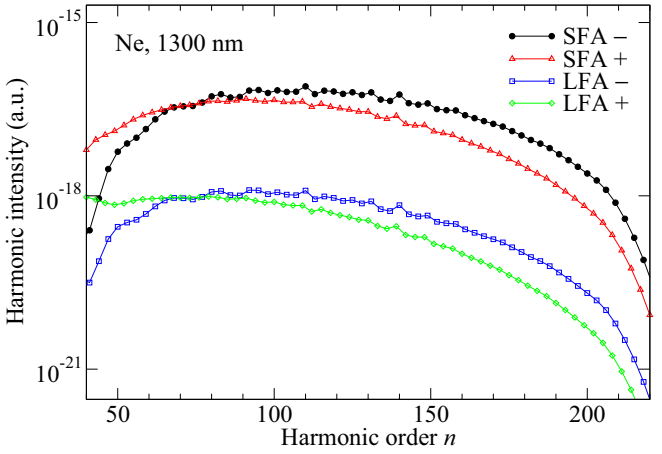

FIG. 9. Harmonic intensity for Ne and bicircular field with component wavelengths 1300 and 650 nm and equal component intensities 4×10^{14} W/cm^2. The two upper curves are obtained using the strong-field approximation, while the two lower curves are calculated in the LFA.

HHG spectra, presented in Fig. 9, do not change qualitatively if we use the LFA instead of the SFA.

V. CONCLUSIONS

The low-frequency approximation, formulated earlier for laser-assisted scattering and high-order above-threshold ionization, is derived for the high-order harmonic generation process. It is a natural extension of the strong-field approximation theory: the SFA plane-wave recombination matrix element is replaced by the exact laser-free recombination matrix element with the momentum of the exact continuum state equal to $\mathbf{k}_s + \mathbf{A}(t)$, where $\mathbf{k}_s$ is the stationary electron momentum, t is the recombination time, and $\mathbf{A}(t) = -\int^t dt' \mathbf{E}(t')$, with $\mathbf{E}(t)$ the electric field vector. In special cases when the rescattering amplitude can be withdrawn in front of the integral over times our LFA reduces to the well-known quantitative rescattering theory. For a linearly polarized laser pulse the validity of the LFA is confirmed by comparison with the results obtained solving the TDSE.

We have applied our LFA to calculate the HHG spectra generated by a bicircular laser field which is presently a hot topic in strong-field physics. We have shown that the numerical calculations can be simplified in the angular momentum basis with the states oriented in the bicircular field component directions (x and y axes).

We have found that the Cooper minimum, which appears at the energy E_q in the photorecombination spectra of Ar atoms, leads to a minimum in the harmonic plateau at the energy $E_q + I_p$, with I_p the ionization potential of Ar. We have also found that for higher harmonic energies the harmonics having helicity -1 are stronger. The jump in asymmetry of left- and right-polarized harmonics appears near the Cooper minimum. The explanation why for higher energies the harmonics having helicity -1 are stronger is given using semiclassical arguments and quantum-orbit theory in Sec. V of Ref. [44]. The mentioned asymmetry remains also in the focal-averaged spectra. This fact can be used to generate an attosecond pulse train of circularly polarized harmonics, as suggested in Ref. [42].

We have also presented the HHG spectra for Ne atoms for which the Cooper minimum is absent. The mentioned asymmetry appears also in this case. However, the asymmetry is stronger for Ar so that HHG by Ar atoms is a better candidate to generate circularly polarized attosecond pulse trains.

[1] A. McPherson, G. Gibson, H. Jara, U. Johann, T. S. Luk, I. A. McIntyre, K. Boyer, and C. K. Rhodes, J. Opt. Soc. Am. B **4**, 595 (1987).

[2] M. Ferray, A. L'Huillier, X. F. Li, L. A. Lompre, G. Mainfray, and C. Manus, J. Phys. B **21**, L31 (1988).

[3] A. L'Huillier, J. Phys. B **50**, 060501 (2017).

[4] P. Salières, A. L'Huillier, Ph. Antoine, and M. Lewenstein, Adv. At. Mol. Opt. Phys. **41**, 83 (1999).

[5] I. P. Christov, M. M. Murnane, and H. C. Kapteyn, Phys. Rev. Lett. **78**, 1251 (1997).

[6] A. Rundquist, C. Durfee, Z. Chang, C. Herne, H. Kapteyn, and M. Murnane, Science **280**, 1412 (1998).

[7] R. A. Bartels, A. Paul, H. Green, H. C. Kapteyn, M. M. Murnane, S. Backus, I. P. Christov, Y. Liu, D. Attwood, and C. Jacobsen, Science **297**, 376 (2002).

[8] J. Itatani, J. Levesque, D. Zeidler, H. Niikura, H. Pépin, J. C. Kieffer, P. B. Corkum, and D. M. Villeneuve, Nature (London) **432**, 867 (2004).

[9] G. Sansone, E. Benedetti, F. Calegari, C. Vozzi, L. Avaldi, R. Flammini, L. Poletto, P. Villoresi, C. Altucci, R. Velotta, S. Stagira, S. De Silvestri, and M. Nisoli, Science **314**, 443 (2006).

[10] E. Goulielmakis, M. Schultze, M. Hofstetter, V. S. Yakovle, J. Gagnon, M. Uiberacker, A. L. Aquila, E. M. Gullikson, D. T. Attwood, R. Kienberger, F. Krausz, and U. Kleineberg, Science **320**, 1614 (2008).

[11] O. Smirnova O. Y. Mairesse, S. Patchkovskii, N. Dudovich, D. Villeneuve, P. Corkum, and M. Y. Ivanov, Nature (London) **460**, 972 (2009).

[12] H. J. Wörner, J. B. Bertrand, D. V. Kartashov, P. B. Corkum, and D. M. Villeneuve, Nature (London) **466**, 604 (2010).

[13] E. Goulielmakis, E. G. Wirth, R. Santra, N. Rohringer, V. S. Yakovlev, S. Zherebtsov, T. Pfeifer, A. M. Azzeer, M. F. Kling, S. R. Leone, and F. Krausz, Nature (London) **466**, 739 (2010).

[14] C. Vozzi, M. Negro, F. Calegari, G. Sansone, M. Nisoli, S. De Silvestri, and S. Stagira, Nat. Phys. **7**, 822 (2011).

[15] P. B. Corkum, Phys. Rev. Lett. **71**, 1994 (1993).

[16] K. C. Kulander, K. J. Schafer, and J. L. Krause, in *Super-Intense Laser-Atom Physics*, NATO Advanced Science Institutes Series Vol. 316, Series B: Physics, edited by B. Piraux, A. L'Huillier, and K. Rzążewski (Plenum, New York, 1993), p. 95.

[17] M. Lewenstein, Ph. Balcou, M. Yu. Ivanov, A. L'Huillier, and P. B. Corkum, Phys. Rev. A **49**, 2117 (1994).

[18] D. B. Milošević and B. Piraux, Phys. Rev. A **54**, 1522 (1996).

[19] D. B. Milošević, W. Becker, and R. Kopold, Phys. Rev. A **61**, 063403 (2000).

[20] T. Morishita, A.-T. Le, Z. Chen, and C. D. Lin, Phys. Rev. Lett. **100**, 013903 (2008); A. T. Le, T. Morishita, and C. D. Lin, Phys. Rev. A **78**, 023814 (2008).

[21] C. D. Lin, A. T. Le, Z. Chen, T. Morishita, and R. Lucchese, J. Phys. B **43**, 122001 (2010).

[22] M. V. Frolov, N. L. Manakov, T. S. Sarantseva, M. Y. Emelin, M. Y. Ryabikin, and A. F. Starace, Phys. Rev. Lett. **102**, 243901 (2009).

[23] N. M. Kroll and K. M. Watson, Phys. Rev. A **8**, 804 (1973).

[24] P. S. Krstić and D. B. Milošević, J. Phys. B **20**, 3487 (1987); D. B. Milošević and P. S. Krstić, *ibid.* **20**, 2843 (1987); **21**, L303 (1988).

[25] D. B. Milošević, J. Phys. B **28**, 1869 (1995); Phys. Rev. A **53**, 619 (1996).

[26] F. Ehlotzky, A. Jaroń, and J. Z. Kamińsky, Phys. Rep. **297**, 63 (1998).

[27] A. Čerkić, E. Hasović, D. B. Milošević, and W. Becker, Phys. Rev. A **79**, 033413 (2009).

[28] D. B. Milošević and F. Ehlotzky, Phys. Rev. A **58**, 3124 (1998).

[29] D. B. Milošević, Phys. Rev. A **90**, 063423 (2014).

[30] C. Chen, Z. Tao, C. Hernández-García, P. Matyba, A. Carr, R. Knut, O. Kfir, D. Zusin, C. Gentry, P. Grychtol, O. Cohen, L. Plaja, A. Becker, A. Jaron-Becker, H. Kapteyn, and M. Murnane, Sci. Adv. **2**, e1501333 (2016).

[31] H. Eichmann, A. Egbert, S. Nolte, C. Momma, B. Wellegehausen, W. Becker, S. Long, and J. K. McIver, Phys. Rev. A **51**, R3414 (1995).

[32] S. Long, W. Becker, and J. K. McIver, Phys. Rev. A **52**, 2262 (1995).

[33] T. Zuo and A. D. Bandrauk, J. Nonlinear Opt. Phys. Mat. **04**, 533 (1995).

[34] O. E. Alon, V. Averbukh, and N. Moiseyev, Phys. Rev. Lett. **80**, 3743 (1998).

[35] W. Becker, B. N. Chichkov, and B. Wellegehausen, Phys. Rev. A **60**, 1721 (1999).

[36] D. B. Milošević and W. Sandner, Opt. Lett. **25**, 1532 (2000); D. B. Milošević, W. Becker, R. Kopold, and W. Sandner, Laser Phys. **11**, 165 (2001).

[37] D. B. Milošević and W. Becker, Phys. Rev. A **62**, 011403(R) (2000); J. Mod. Opt. **52**, 233 (2005).

[38] A. Fleischer, O. Kfir, T. Diskin, P. Sidorenko, and O. Cohen, Nat. Photonics **8**, 543 (2014).

[39] M. Ivanov and E. Pisanty, Nat. Photonics **8**, 501 (2014).

[40] E. Pisanty, S. Sukiasyan, and M. Ivanov, Phys. Rev. A **90**, 043829 (2014).

[41] D. B. Milošević, J. Phys. B **48**, 171001 (2015).

[42] D. B. Milošević, Opt. Lett. **40**, 2381 (2015).

[43] L. Medišauskas, J. Wragg, H. van der Hart, and M. Yu. Ivanov, Phys. Rev. Lett. **115**, 153001 (2015).

[44] D. B. Milošević, Phys. Rev. A **92**, 043827 (2015).

[45] O. Kfir, P. Grychtol, E. Turgut, R. Knut, D. Zusin, D. Popmintchev, T. Popmintchev, H. Nembach, J. M. Shaw, A. Fleischer, H. Kapteyn, M. Murnane, and O. Cohen, Nat. Photonics **9**, 99 (2015).

[46] T. Fan, P. Grychtol, R. Knut, C. Hernández-García, D. D. Hickstein, D. Zusin, C. Gentry, F. J. Dollar, C. A. Mancuso, C. Hogle, O. Kfir, D. Legut, K. Carva, J. L. Ellis, K. Dorney, C. Chen, O. Shpyrko, E. E. Fullerton, O. Cohen, P. M. Oppeneer, D. B. Milošević, A. Becker, A. A. Jaroń-Becker, T. Popmintchev, M. M. Murnane, and H. C. Kapteyn, Proc. Natl. Acad. Sci. USA **112**, 14206 (2015).

[47] D. M. Reich and L. B. Madsen, Phys. Rev. A **93**, 043411 (2016).

[48] D. Baykusheva, M. S. Ahsan, N. Lin, and H. J. Wörner, Phys. Rev. Lett. **116**, 123001 (2016).

[49] H. Du, J. Zhang, S. Ben, H.-Y. Zhong, T.-T. Xu, J. Guo, and X.-S. Liu, Chin. Phys. B **25**, 043202 (2016).

[50] F. Mauger, A. D. Bandrauk, and T. Uzer, J. Phys. B **49**, 10LT01 (2016).

[51] D. M. Reich and L. B. Madsen, Phys. Rev. Lett. **117**, 133902 (2016).

[52] X. Liu, X. Zhu, L. Li, Y. Li, Q. Zhang, P. Lan, and P. Lu, Phys. Rev. A **94**, 033410 (2016).

[53] S. Odžak, E. Hasović, and D. B. Milošević, Phys. Rev. A **94**, 033419 (2016).

[54] E. Hasović, S. Odžak, W. Becker, and D. B. Milošević, Mol. Phys. **115**, 1750 (2017).

[55] S. Odžak, E. Hasović, W. Becker, and D. B. Milošević, J. Mod. Opt. **64**, 971 (2017).

[56] K. M. Dorney, J. L. Ellis, C. Hernández-García, D. D. Hickstein, C. A. Mancuso, N. Brooks, T. Fan, G. Fan, D. Zusin, C. Gentry, P. Grychtol, H. C. Kapteyn, and M. M. Murnane, Phys. Rev. Lett. **119**, 063201 (2017).

[57] D. B. Milošević, J. Phys. B **29**, 875 (1996).

[58] D. B. Milošević, G. G. Paulus, D. Bauer, and W. Becker, J. Phys. B **39**, R203 (2006).

[59] A. F. Starace, *Theory of Atomic Photoionization, Handbuch der Physik* Vol. 31 (Springer, Berlin, 1982), p. 1.

[60] M. Ya. Amusia, *Atomic Photoeffect* (Springer, Berlin, 1990).

[61] J. W. Cooper, Phys. Rev. **128**, 681 (1962); S. T. Manson and J. W. Cooper, *ibid.* **165**, 126 (1968).

[62] S. Minemoto, T. Umegaki, Y. Oguchi, T. Morishita, A.-T. Le, S. Watanabe, and H. Sakai, Phys. Rev. A **78**, 061402(R) (2008).

[63] H. J. Wörner, H. Niikura, J. B. Bertrand, P. B. Corkum, and D. M. Villeneuve, Phys. Rev. Lett. **102**, 103901 (2009).

[64] J. Higuet, H. Ruf, N. Thiré, R. Cireasa, E. Constant, E. Cormier, D. Descamps, E. Mével, S. Petit, B. Pons, Y. Mairesse, and B. Fabre, Phys. Rev. A **83**, 053401 (2011).

[65] A. D. Shiner, B. E. Schmidt, C. Trallero-Herrero, P. B. Corkum, J.-C. Kieffer, F. Légaré, and D. M. Villeneuve, J. Phys. B **45**, 074010 (2012).

[66] S. Bhardwaj, S.-K. Son, K.-H. Hong, C.-J. Lai, F. X. Kärtner, and R. Santra, Phys. Rev. A **88**, 053405 (2013).

[67] D. B. Milošević, W. Becker, M. Okunishi, G. Prümper, K. Shimada, and K. Ueda, J. Phys. B **43**, 015401 (2010).

[68] A. A. Radzig and B. M. Smirnov, *Reference Data on Atoms, Molecules and Ions* (Springer, Berlin, 1985).

[69] *Computational Atomic Physics: Electron and Positron Collisions with Atoms and Ions*, edited by K. Bartschat (Springer, Berlin, 1996).

[70] M. V. Frolov, N. L. Manakov, T. S. Sarantseva, and A. F. Starace, Phys. Rev. A **86**, 063406 (2012).

[71] M. V. Frolov, T. S. Sarantseva, N. L. Manakov, K. D. Fulfer, B. P. Wilson, J. Troß, X. Ren, E. D. Poliakoff, A. A. Silaev, N. V. Vvedenskii, A. F. Starace, and C. A. Trallero-Herrero, Phys. Rev. A **93**, 031403(R) (2016).

[72] T. S. Sarantseva, A. A. Silaev, and N. L. Manakov, J. Phys. B **50**, 074002 (2017).

[73] T. S. Sarantseva, M. V. Frolov, N. L. Manakov, M. Yu. Ivanov, and A. F. Starace, J. Phys. B **46**, 231001 (2013).

[74] The position of the Cooper minimum depends on the used potential $V_s(r)$. Instead of the potential (18) one can use Muller's potential [H. G. Muller, Phys. Rev. A **60**, 1341 (1999)], which shifts the Cooper minimum for Ar to higher photon energies; see C. Jin, A.-T. Le, and C. D. Lin, *ibid.* **79**, 053413 (2009). A more precise position can be obtained by taking into account multielectron effects. The measured value is between 48 and 49 eV. Experiments measure total photoionization cross section and include all possible orientations between the electron momentum and light polarization axis (incoherent process). On the other hand, in HHG, which is a coherent process, specific orientations are preferable (for linear polarization the electron moves along the polarization axis, while for a bicircular field different quantum orbits are preferred). This can also be the reason for the small difference of our result and the experimental position of the Cooper minimum.

[75] R. Kopold, W. Becker, M. Kleber, and G. G. Paulus, J. Phys. B **35**, 217 (2002).